Two chirality classes of ac quantum transport in metallic carbon nanotubes

Takahiro Yamamoto,[1] Kenji Sasaoka,[1] Satoshi Watanabe,[1] and Kazuyuki Watanabe[2]
[1]*Department of Materials Engineering, The University of Tokyo, 7-3-1 Hongo, Bunkyo, Tokyo 113-8656, Japan*
[2]*Department of Physics, Tokyo University of Science, 1-3 Kagurazaka, Shinjuku, Tokyo 162-8601, Japan*
(Received 27 November 2009; revised manuscript received 2 March 2010; published 25 March 2010)

We report a theoretical investigation of the ac transport in metallic single-walled carbon nanotubes (SWNTs). In contrast to the dc conductance, we clarify that the ac admittance behavior of finite-length metallic SWNTs does depend on the tube chirality and it is classified into two chirality categories: that of metals 1 (e.g., metallic zigzag SWNTs) and 2 (e.g., armchair SWNTs). Moreover, we find that for long SWNTs the admittances of both metals 1 and 2 behave as a simple series circuit consisting of a half of the quantum resistance and a half of the quantum inductance.

DOI: 10.1103/PhysRevB.81.115448 PACS number(s): 73.63.−b, 85.35.Kt

I. INTRODUCTION

Carbon nanotubes (CNTs) can be metallic or semiconducting depending on their chirality.[1,2] Semiconducting CNTs are potential candidates for field effect transistors due to their high electrical mobility,[3] and metallic CNTs are considered as interconnects in future large-scale integrated circuits due to large allowable current.[4] Toward the realization of practical CNT electronics, a considerable amount of effort has been devoted to the investigation of the dc electronic transport in CNTs.[5] In addition to the dc transport, the ac transport is a key issue for designing and controlling ultrafast CNT-based devices.[6] Nevertheless, there have been a few reports on the ac transport in CNTs until recently.

The ac response of CNTs has been measured in wide frequency ranges from kilohertz to terahertz by several experimental groups.[6–12] A recent experiment showed that the terahertz-frequency electron response of quasimetallic single-walled CNTs (SWNTs) is dominated by ballistic propagation of single-particle excitations rather than collective plasmon modes.[12] The ac transport properties of CNTs have also been theoretically investigated, focusing particularly on extremely high frequency regimes (subpetahertz regime).[13,14] These theoretical studies showed that the displacement current contributes largely to the admittance behavior of CNTs under such high frequency regimes,[13] although it is negligible for usual bulk materials. However, there is a wide gap between frequency regimes explored by theories and experiments, and the characteristic features of terahertz response, which are important for next-generation CNT-based devices, have not been clarified yet. Most recently, Kienle and Léonard theoretically investigated the effects of terahertz ac gate-voltage modulation on CNT-based field effect transistor characteristics,[15] but the effects of terahertz ac source-drain voltage remain to be elucidated. This paper reports an atomistic simulation of the coherent quantum transport in metallic SWNTs under terahertz ac source-drain voltage, focusing on the chirality dependence of admittance.

The paper is organized as follows. In Sec. II, we explain general properties of admittance of multiterminal systems consisting of a central region connected to multiple leads, and we introduce the nonequilibrium Green's function (NEGF) description of the admittance of multiterminal systems. In Sec. III, the NEGF simulation results are presented (Sec. III A) and the obtained NEGF results are analyzed using a classical equivalent circuit (Sec. III B). Moreover, the results obtained from the NEGF simulations and the equivalent circuit analysis are explained by a low-energy effective model taking into account only two linear energy bands crossing the Fermi level of metallic SWNTs (Sec. III C). In Sec. IV, we conclude that the ac admittance behavior of finite-length metallic SWNTs does depend on the tube chirality and it is classified into two chirality categories: that of metals 1 (e.g., metallic zigzag SWNTs) and 2 (e.g., armchair SWNTs). The paper is finally summarized in Sec. V.

II. THEORETICAL AND NUMERICAL METHODOLOGIES

Our target system is a two-terminal system consisting of a metallic SWNT embedded in a cylindrical source and drain electrodes, as shown in Fig. 1. This system can be modeled by dividing an infinitely long SWNT into three parts: a central device region with N unit cells and the semi-infinite left and right parts attached to the metallic electrodes, i.e., a finite-length SWNT coupled seamlessly to two SWNT leads of the same type. This model is valid for a ballistic transport where the contact resistance at the interfaces between a SWNT and electrodes is much less than the quantum resistance h/e^2. In fact, the embedded contact geometry has a small contact resistance in comparison with that of tube-on-metal and metal-on-tube geometries. Our simulation method is based on the NEGF technique within the wideband-limit approximation[16–18] combined with a nearest-neighbor π-orbital tight-binding model. We use $t_0=-2.75$ eV as the hopping integral between π orbitals.[13]

We now explain the general properties of admittance of a multiterminal system. The electronic current flowing from

FIG. 1. (Color online) Schematic of the cross section of a cylindrical SWNT device.

the device region to the α lead is expressed as $J_\alpha(t) = \mathrm{Re}[J_\alpha(\omega)e^{-i\omega t}]$ with

$$J_\alpha(\omega) = \sum_\beta Y_{\alpha\beta}(\omega)V_\beta(\omega), \tag{1}$$

where $V_\beta(\omega)$ is the amplitude of the harmonic time-varying voltage applied to the β lead and $Y_{\alpha\beta}(\omega)$ is the admittance between α and β leads. The admittance $Y_{\alpha\beta}(\omega)$ is divided into two parts associated with the conduction current and the displacement current,

$$Y_{\alpha\beta}(\omega) = Y^c_{\alpha\beta}(\omega) + P_\alpha Y^d_\beta(\omega). \tag{2}$$

The partition coefficients P_α satisfy relations $\Sigma_\alpha P_\alpha = 1$ and $P_\alpha = -\Sigma_\gamma Y^c_{\alpha\gamma}(\omega)/\Sigma_\gamma Y^d_\gamma(\omega)$ from two physical requirements: current conservation $[\Sigma_\alpha Y_{\alpha\beta}(\omega) = 0]$ and the gauge invariance $[\Sigma_\beta Y_{\alpha\beta}(\omega) = 0]$.[19] For two-terminal systems of interest here, the two requirements give a relation among the admittance elements, $Y(\omega) \equiv Y_{LR}(\omega) = Y_{RL}(\omega) = -Y_{LL}(\omega) = -Y_{RR}(\omega)$, where L (R) denotes the left (right) lead.

Next, we briefly review the NEGF description of the admittance of a multiterminal system. Within a linear-response approximation with respect to applied voltages, the conduction-current admittance $Y^c_{\alpha\beta}(\omega)$ is expressed as

$$Y^c_{\alpha\beta}(\omega) = \frac{e^2}{h}\int_{-\infty}^{\infty} d\epsilon \frac{f_\alpha(\epsilon) - f_\beta(\epsilon + \hbar\omega)}{\hbar\omega} T_{\alpha\beta}(\epsilon, \omega). \tag{3}$$

Here, $f_\alpha(\epsilon)$ is the Fermi-Dirac distribution function of the α lead and $T_{\alpha\beta}(\epsilon, \omega)$ is a transmission function under the ac-bias voltage with frequency ω, which is given by

$$T_{\alpha\beta}(\epsilon, \omega) = \mathrm{Tr}[\boldsymbol{G}(\epsilon + \hbar\omega)\boldsymbol{\Gamma}_\beta \boldsymbol{G}^\dagger(\epsilon)\boldsymbol{\Gamma}_\alpha] - i\delta_{\alpha\beta}\,\mathrm{Tr}[\boldsymbol{G}(\epsilon + \hbar\omega)\boldsymbol{\Gamma}_\alpha - \boldsymbol{\Gamma}_\alpha \boldsymbol{G}^\dagger(\epsilon)], \tag{4}$$

in terms of the Green's functions. Here, $\boldsymbol{G}(\omega)$ and $\boldsymbol{\Gamma}_\alpha$ are the retarded Green's function and the level broadening function, respectively. In the dc limit $(\omega \to 0)$, the conduction-current admittance expression in Eq. (3) reduces to the well-known Landauer formula for the dc transport.[20] On the other hand, the displacement-current admittance $Y^d_\beta(\omega)$ is given by

$$Y^d_\beta(\omega) = \frac{e^2}{h}\int_{-\infty}^{\infty} d\epsilon [f_\beta(\epsilon) - f_\beta(\epsilon + \hbar\omega)] Y^d_\beta(\epsilon, \omega), \tag{5}$$

where the energy-resolved admittance $Y^d_\beta(\epsilon, \omega)$ is expressed as

$$Y^d_\beta(\epsilon, \omega) = -i\,\mathrm{Tr}[\boldsymbol{G}(\epsilon + \hbar\omega)\boldsymbol{\Gamma}_\beta \boldsymbol{G}^\dagger(\epsilon)], \tag{6}$$

in terms of the Green's functions. In the dc limit, the displacement-current admittance in Eq. (5) goes to zero, $Y^d_\beta(0) = 0$.

In addition to the above-mentioned intrinsic admittance of SWNTs, the parasitic admittance is often dominant in the measurements of nanoscale objects with the ac voltage up to terahertz. However, it should be possible to significantly reduce the parasitic admittance by a detailed electrode geometry design or by using the nanotube itself as interconnect electrodes.[21] Therefore, we focus only on the intrinsic admittance of SWNTs in the following sections.

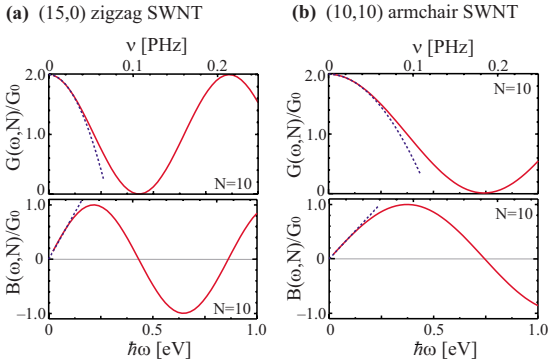

FIG. 2. (Color online) The conductance $G(\omega, N)$ and susceptance $B(\omega, N)$ of the (15,0) zigzag and the (10,10) armchair SWNTs with $N = 10$. N is the number of the unit cells in the central region and $G_0 = e^2/h$ is the conductance quantum. Blue dashed curves represent the low-frequency behavior of the conductance $[G(\omega, N) = 2G_0 - \alpha(N)\omega^2]$ and the susceptance $[B(\omega, N) = \beta(N)\omega]$.

In this section, we presented a general expression of the admittance in terms of the Green's functions. The NEGF method is a powerful tool not only for calculating the admittance but also for simulating various physical quantities. For example, we discuss the nonequilibrium electron density of metallic SWNTs under the ac-bias voltages in the Appendix.

III. NUMERICAL RESULTS AND THEORETICAL ANALYSES

A. NEGF simulations of admittance

The metallic SWNTs satisfy a condition $\mathrm{mod}(2n + m, 3) = 0$, where (n, m) is the chiral index that specifies the structure of SWNT.[1,2] The conductance $G(\omega, N)$ (real part of the admittance) and the susceptance $B(\omega, N)$ (imaginary part of the admittance) of the (15,0) zigzag and the (10,10) armchair SWNTs with $N = 10$ unit cells are represented in Figs. 2(a) and 2(b), respectively. In the dc limit $\omega \to 0$, the conductance is $G(0, N) = 2G_0$ for both (15,0) and (10,10) SWNTs since metallic SWNTs have two conduction channels at the Fermi level $\epsilon_F = 0$, where $G_0 = e^2/h$ is the quantum conductance. With increasing frequency from zero, the conductances oscillate and the susceptances repeat transitions between the inductive $(B > 0)$ and capacitive $(B < 0)$ behaviors. The oscillation and transition in the subpetahertz frequency regime was already discussed by a previous theoretical work[14] and our results are in good agreement with it.

In this work, we pay attention to the lower-frequency behavior of $G(\omega, N)$ and $B(\omega, N)$. Here, "low-frequency" means that ω is much smaller than an inverse of dwell time τ_d^{-1} that an electron stays inside the central device region of a SWNT. For example, such a low-frequency regime is estimated as $\omega < 1$ THz for 1-μm-length metallic SWNTs. In the low-frequency regime, the conductance and the susceptance of both the (15,0) and (10,10) SWNTs behave as

$$G(\omega, N) = 2G_0 - \alpha(N)\omega^2, \tag{7}$$

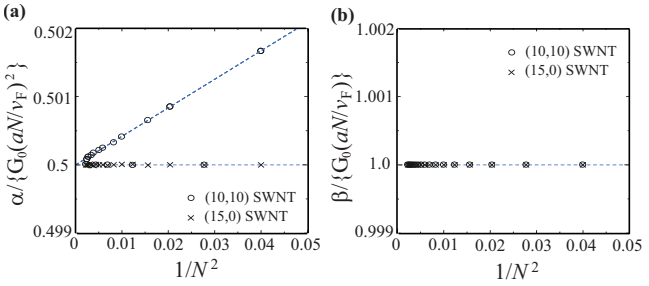

FIG. 3. (Color online) (a) $\alpha(N)/\{G_0(aN/v_F)^2\}$ and (b) $\beta(N)/\{G_0(aN/v_F)\}$ of the (15,0) SWNT (cross marks) and the (10,10) SWNT (open circles) as functions of $1/N^2$, where v_F is the Fermi velocity and a is the unit-cell length of SWNT.

$$B(\omega,N) = \beta(N)\omega, \tag{8}$$

as shown by the dashed curves in Fig. 2. These relationships have been observed not only in the (15,0) and (10,10) SWNTs, but also in all metallic SWNTs we have calculated. These relationships are not unique properties of SWNTs but are general properties originating from the fact that $G(\omega,N)$ and $B(\omega,N)$ are the even and odd functions of ω, respectively. Thus, every characteristic of SWNTs such as chirality dependence incorporates into $\alpha(N)$ and $\beta(N)$. Figure 3 shows $\alpha(N)/\{G_0(aN/v_F)^2\}$ and $\beta(N)/\{G_0(aN/v_F)\}$ of the (15,0) SWNT (cross marks) and the (10,10) SWNT (open circles) as functions of $1/N^2$, where $v_F=10^6$ m/s is the Fermi velocity and a is the unit-cell length of SWNT (e.g., $a=4.32$ Å for zigzag SWNTs and $a=2.49$ Å for armchair ones). $\alpha(N)/\{G_0(aN/v_F)^2\}$ of the (10,10) SWNT exhibits a remarkable length dependence, whereas that of the (15,0) SWNT is constant with the tube length. On the other hand, $\beta(N)/\{G_0(aN/v_F)\}$ is constant in both cases. A central aim of the following discussion is to clarify the physical origin of these admittance behaviors.

B. Equivalent circuit analysis

Now, we seek a classical equivalent circuit describing the above-mentioned relationships, $G(\omega,N)=2G_0-\alpha(N)\omega^2$ and $B(\omega,N)=\beta(N)\omega$. This is a challenging problem of how to incorporate the quantum feature of the ac transport in metallic SWNTs into circuit components. As such an equivalent circuit, we introduce a parallel circuit of R_c-L and R_q-C series circuits shown in Fig. 4. In fact, the low-frequency conductance and susceptance of the equivalent circuit are expressed as

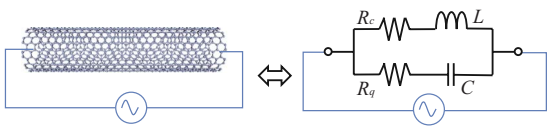

FIG. 4. (Color online) The equivalent circuit for metallic single-walled carbon nanotubes. The low-frequency ac response of SWNTs is described by a classical equivalent circuit consisting of a parallel circuit of R_c-L and R_q-C series circuits. L and C are an inductance and a capacitance, respectively. R_c and R_q are the contact resistance and the charge relaxation resistance, respectively.

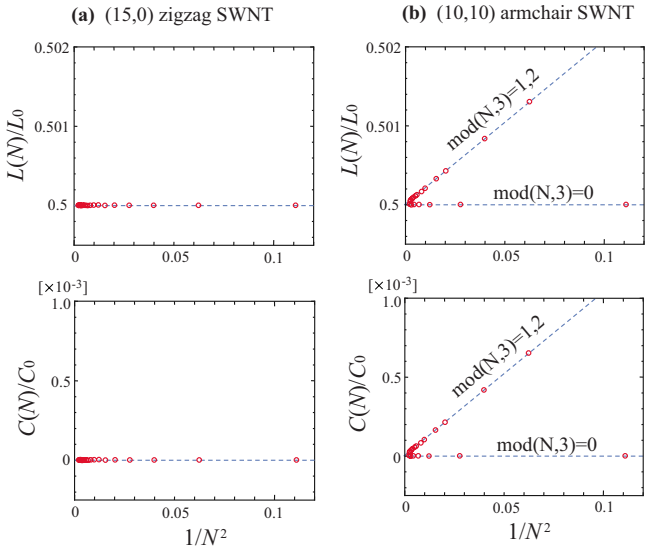

FIG. 5. (Color online) (a) The inductance $L(N)$ and the capacitance $C(N)$ of the (15,0) SWNT as functions of $1/N^2$. (b) $L(N)$ and $C(N)$ of the (10,10) SWNT as functions of $1/N^2$. L_0 and C_0 are the quantum inductance and the quantum capacitance, respectively (see the text). The circles denote the simulation results and the dashed lines are given by Eqs. (13) and (14) in the text.

$$G(\omega,N) = \frac{1}{R_c} - \left(\frac{L^2}{R_c^3} - R_q C^2\right)\omega^2, \tag{9}$$

$$B(\omega,N) = \left(\frac{L}{R_c^2} - C\right)\omega, \tag{10}$$

up to the second order of ω. Here, R_c and R_q are the contact resistance[20] and the charge relaxation resistance,[22,23] respectively. For pristine metallic SWNTs, both the contact and the charge relaxation resistances are given by a half of quantum resistance, that is, $R_c=R_q=h/2e^2$. On the other hand, the inductance L and the capacitance C in the equivalent circuit are determined by comparing Eqs. (9) and (10) to the above-obtained NEGF data of $\alpha(N)$ and $\beta(N)$.

A similar equivalent circuit was first introduced intuitively by Cuniberti *et al.* for fitting the numerical data of the admittance of quantum wire[24] and the validity of the circuit was confirmed analytically by Yam *et al.* only for the conduction-current admittance in a simple model: two-site system in contact with the left and right electrodes.[25] In the last part of this paper, we will analytically establish the equivalent circuit in Fig. 4 for metallic SWNTs, taking into account of both the conduction-current admittance and the displacement-current admittance. Before doing that we discuss the results obtained by analyzing the NEGF data using the equivalent circuit in Fig. 4.

Figures 5(a) and 5(b) show $L(N)/L_0$ and $C(N)/C_0$ for the (15,0) and (10,10) SWNTs as functions of $1/N^2$, respectively. Here, L_0 is the quantum inductance $L_0=\tau_d R_c$ related to the dwell time τ_d (Ref. 26) and C_0 is the quantum capacitance $C_0=e^2D(\epsilon_F)$ described by the density of states (DOS) $D(\epsilon_F)$ at the Fermi level.[27] For metallic SWNTs with length Na, L_0 and C_0 are given by

$$L_0 = \frac{h}{2e^2}\frac{Na}{v_F} = (12.9\ \text{nH}/\mu\text{m})Na, \tag{11}$$

$$C_0 = \frac{4e^2}{h}\frac{Na}{v_F} = (155\ \text{aF}/\mu\text{m})Na. \tag{12}$$

For the (15,0) SWNT, the inductance equals to a half of the quantum inductance and the capacitance is always zero: $L(N)=L_0/2$ and $C(N)=0$. This behavior has been observed not only for the (15,0) SWNT, but also for all zigzag SWNTs we have calculated. Thus, we conclude that the low-frequency admittance of the zigzag SWNTs is described by a simple series circuit consisting of $R_L=1/(2G_0)$ and $L=L_0/2$. Since the dwell time is give by $\tau_d=Na/v_F$, the inductance $L=\tau_d R_c$ increases in proportion to N.

As seen in Fig. 5(b), the length dependences of the inductance and the capacitance of the (10,10) SWNT are significantly different from that of the zigzag SWNTs. For $\text{mod}(N,3)=0$, $L(N)$ is always a half of the quantum inductance and $C(N)$ is always zero. This R_c-L series circuit behavior is the same as the zigzag-SWNT case. On the contrary, for $\text{mod}(N,3)\neq 0$, $L(N)/L_0$ goes to 1/2 in proportion to $1/N^2$, and $C(N)/C_0$ is not zero for finite N and disappears in proportion to $1/N^2$. Thus, the admittances of the metallic zigzag and the armchair SWNTs behave as a series circuit consisting of $R=1/(2G_0)$ and $L(N)=L_0/2$ in the large-N limit. These numerical results are summarized as follows:

$$L(N) = \left(\frac{1}{2} + \frac{A}{N^2}\right)L_0, \tag{13}$$

$$C(N) = \frac{A}{2N^2}C_0, \tag{14}$$

where $A=0$ for the metallic zigzag SWNTs and the armchair SWNTs with $\text{mod}(N,3)=0$, and $A\neq 0$ for the armchair ones with $\text{mod}(N,3)\neq 0$.

C. Low-energy effective model

The above results obtained from the NEGF simulations and the equivalent circuit analysis can be explained by a low-energy effective model taking into account only two linear energy bands crossing the Fermi level. The linear band approximation works well in the low-frequency regime below terahertz where the trigonal warping effect is negligible.[28] According to the linear band model, the retarded Green's function for an armchair SWNT at the K point is expressed as

$$G_{\xi,\zeta;\xi',\zeta'}(\epsilon_F) = -i\frac{a}{\hbar v_F}\frac{e^{2i\pi(\zeta-\zeta')}}{2n}e^{-ik_F a|\xi-\xi'|}, \tag{15}$$

where the indices (ξ,ζ) identify the position on graphene's unit cell on the tube's cylindrical coordinates (see Fig. 6). The Green's function at the K' point can be obtained by replacing $k_F(=2\pi/3a)$ with $-k_F$ in Eq. (15). The level broadening function of the left (right) lead is given by

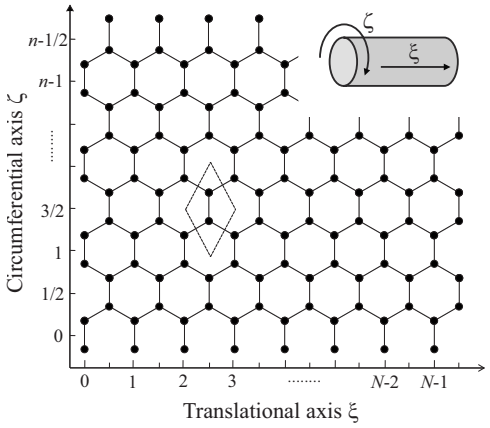

FIG. 6. The unrolled (n,n)-armchair SWNT with length Na. The horizontal axis ξ is along the translational direction and the vertical axis ζ is along the circumferential direction (see also the inset). The graphene unit cell including two carbon atoms is represented by the dotted rhombus and its position is identified by the indices (ξ,ζ).

$$\Gamma^{L(R)}_{\xi,\zeta;\xi',\zeta'} = \begin{cases} \dfrac{2}{n}\dfrac{\hbar v_F}{a}, & \xi,\xi'=0 \quad (\xi,\xi'=N-1/2) \\ 0, & \text{otherwise}, \end{cases} \tag{16}$$

where n is a chiral index. Expanding the admittance $Y_{\alpha\beta}(\omega,N)$, which was introduced in the Introduction, up to the second order of ω, and then substituting Eqs. (15) and (16) into the expanded form of $Y_{\alpha\beta}(\omega,N)$, we obtain the low-frequency expressions of the conductance $G(\omega,N)$ and the susceptance $B(\omega,N)$,

$$\frac{G(\omega,N)}{G_0} \approx 2 - 2\left[\left(\frac{aN}{2v_F}\right)^2 + A\left(\frac{a}{v_F}\right)^2\right]\omega^2, \tag{17}$$

$$\frac{B(\omega,N)}{G_0} \approx \frac{aN}{v_F}\omega, \tag{18}$$

where

$$A = \frac{1+\cos(k_F a)}{2}\left|\sum_{l=1}^{N}\exp(2ik_F a l)\right|^2 = \begin{cases} 0 & [\text{mod}(N,3)=0] \\ 1/48 & [\text{mod}(N,3)=1 \text{ and } 2]. \end{cases} \tag{19}$$

Comparing Eqs. (17) and (18) to Eqs. (9) and (10), we obtain $R_c=R_q=1/(2G_0)$ and Eqs. (13) and (14). Thus, based on the linear band model, we can explain the capacitance behavior of the armchair SWNTs in Fig. 5(b). The capacitance behavior is determined by the value of A, according to Eq. (14). As seen in Eq. (19), when the multiples of wavelength match the tube length [i.e., $\text{mod}(N,3)=0$], the capacitance is zero. On the other hand, when $\text{mod}(N,3)=1,2$, the capacitance is finite for small-N armchair SWNTs and it disappears with increasing N since the wavelength mismatch becomes negligible as N increases. Using the linear band model, we can also explain that the metallic zigzag SWNTs show $A=0$ independent of N. This is because the multiples of wavelength

of metallic zigzag SWNTs always match the tube length.

Before closing this section, we mention the measurement accuracy required to identify the chirality of SWNTs experimentally from the inductance L and the capacitance C in the equivalent circuit of SWNTs, on the basis of the results obtained from the above effective model. L and C are determined by comparing Eqs. (9) and (10) to α in Eq. (7) and β in Eq. (8), respectively. In order to identify the chirality dependence on L and C in experiments, we have to measure α especially with high accuracy. More strictly speaking, the accuracy of conductance measurements, ΔG, should be high enough to identify the difference between the two dashed curves in Fig. 3(a), $\Delta\alpha$, because ΔG is given by $\Delta G = \Delta\alpha\omega^2$. Since $\Delta\alpha$ is given by $\Delta\alpha = 2AG_0(a/v_F)^2 = (3.18 \times 10^{-9}\ \mathrm{ps}^2)G_0$ from Eqs. (17)–(19), the accuracy ΔG is estimated as $\Delta G \sim 10^{-6}G_0$ for the frequency of a few terahertz, which is comparable to the accuracy of cutting-edge conductance measurements.[29] In addition, it should be noted that the length of SWNTs does not affect the accuracy ΔG required to identify the chirality by measuring L and C because $\Delta\alpha$ is independent of the length. Thus, we emphasize that the chirality of metallic SWNTs with arbitrary length can be identified by the terahertz response measurements.

IV. TWO CHIRALITY CLASSES OF ADMITTANCE BEHAVIOR

Thus far, we have discussed the metallic zigzag $(n,0)$ and the armchair (n,n) SWNTs as typical examples of metallic SWNTs. Now let us generalize our discussion to metallic chiral SWNTs satisfying $\mathrm{mod}(2n+m,3)=0$. Furthermore, the metallic SWNTs can be classified into two categories: metals 1 and 2 obeying $\mathrm{mod}(3m/d_R,3)=0$ and $\mathrm{mod}(3m/d_R,3)\neq 0$, respectively.[30] Here, d_R is the greatest common divisor of $(2m+n)$ and $(2n+m)$. For example, the metallic zigzag SWNTs and the armchair ones are categorized into metals 1 and 2, respectively. A remarkable difference between metals 1 and 2 is a position of the Fermi wave number k_F: the Fermi point is located at $k_F=0$ for metal 1 and is located at $k_F = \pm 2\pi/3a$ for metal 2. Thus far, little attention has been given to the difference between the electronic transport properties of metals 1 and 2, because the DOSs near the Fermi level are the same for all metallic SWNTs (at least within the π-orbital approximation). However, in sharp contrast to the dc conductance, the ac admittance behavior of finite-length metallic SWNTs depends on the chirality and is classified into metals 1 and 2. In fact, the admittance of the (6,3) SWNT belonging to metal 1 exhibits similar behavior as that of the zigzag SWNTs in Fig. 5(a), whereas the admittance of the (8,2) SWNT belonging to metal 2 shows similar behavior as that of the armchair SWNTs in Fig. 5(b). This remarkable chirality dependence of admittance clearly differs from the dc conductance.

V. SUMMARY

In summary, we have investigated the ac quantum transport in metallic SWNTs within the NEGF simulation method in the context of π-orbital tight-binding model. By analyzing the NEGF data using the equivalent circuit model, we found that the ac admittance behavior exhibits a remarkable chirality dependence, which differs significantly from the dc conductance. This result shows that admittance measurement is a potentially useful tool for a chirality identification of metallic SWNTs. In this paper, the discussion has been restricted to pristine SWNTs without defect scattering, boundary scattering, and so on. It is experimentally possible to realize such an ideal situation and to observe nearly quantum conductance ($\sim 2G_0$) by dc transport measurements.[31] When the contact between a SWNT and electrodes is not ideal, the scattering at the contact will influence the ac response of SWNT devices. The NEGF simulation method and the equivalent circuit analysis used in the present study are useful to understand contact effect and other scattering effects on the ac response of various nanostructures, not just of SWNTs.

ACKNOWLEDGMENTS

We would like to thank Tomofumi Tada for reading the draft and making a number of valuable comments. T.Y. acknowledges support from the Ministry of Education, Culture, Sports, Science and Technology (MEXT) of Japan through Grants-in-Aid (Grants No. 19710083 and No. 20048008). This work was also supported in part by the Specific Area Research "Carbon Nanotube Nano-Electronics" and by the Global Center of Excellence (G-COE) Program "Global Center of Excellence for Mechanical Systems Innovation," MEXT of Japan.

APPENDIX: NONEQUILIBRIUM ELECTRON DENSITY UNDER TERAHERTZ ac-BIAS VOLTAGES

On the basis of the NEGF method for the ac transport, we can calculate straightforwardly not only the admittance but also various time-dependent local quantities, such as the current density, the electron distribution, and so on. For example, the difference between the numbers of electrons on the jth atom before and after applying the ac-bias voltage with angular frequency ω, $\delta n_j(t;\omega)$, is expressed as

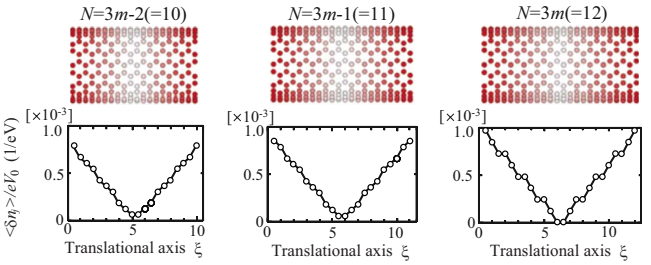

FIG. 7. (Color online) The RMS of the difference between the number of electrons of the (10,10) SWNTs with $N=3m-2(=10)$, $3m-1(=11)$, and $3m(=12)$ before and after applying the 1.0 THz ac-bias voltage. The chemical potentials of the left and right electrodes are given by $\mu_L=-\mu_R=(eV_0/2)\cos(\omega t)$.

$$\delta n_j(t;\omega) = \sum_{\alpha=L,R} \mu_\alpha \int_{-\infty}^{\infty} d\epsilon \frac{f_\alpha(\epsilon) - f_\alpha(\epsilon+\hbar\omega)}{\hbar\omega} \times \mathrm{Re}[\{\boldsymbol{G}(\epsilon+\hbar\omega)\boldsymbol{\Gamma}_\alpha \boldsymbol{G}^\dagger(\epsilon)\}_{jj} \exp(-i\omega t)], \tag{A1}$$

within the linear-response and wideband-limit approximations. Here, $\mu_{L/R}$ is the chemical potential of the left/right electrode.

We now consider $\delta n_j(t;\omega)$ under terahertz ac-bias voltage given by $\mu_L = -\mu_R = (eV_0/2)\cos(\omega t)$. Figure 7 shows the root mean square (RMS) of $\delta n_j(t;\omega)$,

$$\langle \delta n_j(\omega) \rangle = \sqrt{\frac{1}{T}\int_0^T [\delta n_j(t;\omega)]^2 dt}, \tag{A2}$$

of the (10,10) SWNTs for $N=3m-2$, $3m-1$, and $3m$, where $T=2\pi/\omega$ is the period of the ac-bias voltage with frequency $f=2\pi/\omega=1.0$ THz. As seen in Fig. 7, $\langle \delta n_j(\omega) \rangle$ exhibits a three-layer structure along the translational axis of the SWNT that originates from the wavelength of Bloch functions at the Fermi level. The appearance of the three-layer structure is independent of whether the effective capacitance is zero (for $N=3m$) or not (for $N=3m-1$ and $3m-2$).

[1] N. Hamada, S. I. Sawada, and A. Oshiyama, Phys. Rev. Lett. **68**, 1579 (1992).
[2] R. Saito, M. Fujita, G. Dresselhaus, and M. S. Dresselhaus, Appl. Phys. Lett. **60**, 2204 (1992).
[3] S. J. Tans, A. R. M. Verschueren, and C. Dekker, Nature (London) **393**, 49 (1998).
[4] Z. Yao, C. L. Kane, and C. Dekker, Phys. Rev. Lett. **84**, 2941 (2000).
[5] M. J. Biercuk, S. Ilani, C. M. Marcus, and P. L. McEuen, in *Carbon Nanotubes: Advanced Topics in the Synthesis, Structure, Properties and Applications*, edited by A. Jorio, G. Dresselhaus, and M. S. Dresselhaus (Springer, Berlin, 2008), p. 455, and references therein.
[6] Z. Chen, J. Appenzeller, Y.-M. Lin, J. Sippel-Oakley, A. G. Rinzler, J. Tang, S. J. Wind, P. M. Solomon, and P. Avouris, Science **311**, 1735 (2006).
[7] Z. Yu and P. J. Burke, Nano Lett. **5**, 1403 (2005).
[8] Y.-P. Zhao, B. Q. Wei, P. M. Ajayan, G. Ramanath, T.-M. Lu, G.-C. Wang, A. Rubio, and S. Roche, Phys. Rev. B **64**, 201402(R) (2001).
[9] M. Tsutsui, K. Kuno, S. Kurokawa, and A. Sakai, e-J. Surf. Sci. Nanotechnol **5**, 12 (2007).
[10] S. C. Jun, X. M. H. Huang, S. Moon, H. J. Kim, J. Hone, Y. W. Jin, and J. M. Kim, New J. Phys. **9**, 265 (2007).
[11] M. Zhang, X. Huo, and P. C. H. Chan, Appl. Phys. Lett. **88**, 163109 (2006).
[12] Z. Zhong, N. M. Gabor, J. E. Sharping, A. L. Gaeta, and P. L. McEuen, Nat. Nanotechnol. **3**, 201 (2008).
[13] C. Roland, M. Buongiorno Nardelli, J. Wang, and H. Guo, Phys. Rev. Lett. **84**, 2921 (2000).
[14] Y. He, D. Hou, X. Liu, C. Fan, and R. Han, J. Phys.: Condens. Matter **18**, 8707 (2006).
[15] D. Kienle and F. Léonard, Phys. Rev. Lett. **103**, 026601 (2009).
[16] H. Haug and A.-P. Jauho, *Quantum Kinetics in Transport and Optics of Semiconductors* (Springer, Berlin, 1996).
[17] M. P. Anantram and S. Datta, Phys. Rev. B **51**, 7632 (1995).
[18] B. Wang, J. Wang, and H. Guo, Phys. Rev. Lett. **82**, 398 (1999).
[19] M. Büttiker, A. Prêtre, and H. Thomas, Phys. Rev. Lett. **70**, 4114 (1993).
[20] S. Datta, *Electronic Transport in Mesoscopic Systems* (Cambridge University Press, New York, 1995).
[21] P. J. Burke, Solid-State Electron. **48**, 1981 (2004).
[22] M. Büttiker, H. Thomas, and A. Prêtre, Phys. Lett. A **180**, 364 (1993).
[23] Y. M. Blanter, F. W. J. Hekking, and M. Büttiker, Phys. Rev. Lett. **81**, 1925 (1998).
[24] G. Cuniberti, M. Sassetti, and B. Kramer, Phys. Rev. B **57**, 1515 (1998).
[25] C. Yam, Y. Mo, F. Wang, X. Li, G. H. Chen, X. Zheng, Y. Matsuda, J. Tahir-Kheli, and W. A. Goddard III, Nanotechnology **19**, 495203 (2008).
[26] Y. Fu and S. C. Dudley, Phys. Rev. Lett. **70**, 65 (1993).
[27] S. Luryi, Appl. Phys. Lett. **52**, 501 (1988).
[28] T. Ando, J. Phys. Soc. Jpn. **74**, 777 (2005).
[29] E. Lörtscher, H. B. Weber, and H. Riel, Phys. Rev. Lett. **98**, 176807 (2007).
[30] R. Saito, G. Dresselhaus, and M. S. Dresselhaus, *Physical Properties of Carbon Nanotubes* (Imperial College Press, London, 1998).
[31] J. Kong, E. Yenilmez, T. W. Tombler, W. Kim, H. Dai, R. B. Laughlin, L. Liu, C. S. Jayanthi, and S. Y. Wu, Phys. Rev. Lett. **87**, 106801 (2001).